Journal of Zhejiang University-SCIENCE A (Applied Physics & Engineering)
ISSN 1673-565X (Print); ISSN 1862-1775 (Online)
www.jzus.zju.edu.cn; www.springerlink.com
E-mail: jzus@zju.edu.cn

Characterization of spatial variability with observed responses: application of displacement back estimation*

Yi-xuan SUN[1,2], Lu-lu ZHANG[†‡1,2], Hao-qing YANG[1,2], Jie ZHANG[3], Zi-jun CAO[4], Qi CUI[1,2], Jun-yi YAN[5]

[1]*State Key Laboratory of Ocean Engineering, Department of Civil Engineering, Shanghai Jiao Tong University, Shanghai 200092, China*

[2]*Collaborative Innovation Center for Advanced Ship and Deep-Sea Exploration, Shanghai 200092, China*

[3]*Key Laboratory of Geotechnical and Underground Engineering of Ministry of Education, Department of Geotechnical Engineering, Tongji University, Shanghai 200092, China*

[4]*State Key Laboratory of Water Resources and Hydropower Engineering Science, Key Laboratory of Rock Mechanics in Hydraulic Structural Engineering (Ministry of Education), Wuhan University, Wuhan 430072, China*

[5]*Institute of Science and Technology, China Three Gorges Corporation, Beijing 100038, China*

[†]E-mail: lulu_zhang@sjtu.edu.cn

Received Dec. 5, 2019; Revision accepted Feb. 23, 2020; Crosschecked May 13, 2020

Abstract: Soil spatial variability is difficult to evaluate due to insufficient test data. An alternative option is estimation by indirect methods such as inverse analysis. In this paper, two examples are presented to demonstrate the capability and accuracy of the probabilistic estimation method to characterize soil spatial variability with displacement responses. The first example is a soil slope subject to a surcharge load, in which the spatially varied field of the elastic modulus is estimated with displacements. The results show that estimations based on horizontal displacements were more accurate than those based on vertical displacements. The accuracy of the estimated field was substantially reduced by increasing variance of elastic modulus. However, the estimation was generally acceptable as the error was not more than 10%, even for the high variance case (COV_E=1.5). The accuracy of estimation was also affected by the type of covariance function and the correlation length. When the correlation length decreased, the accuracy of estimation was reduced. The second example is a validation of laboratory model tests where a horizontal load was applied on a layered ground. The estimated thicknesses of soil layers were close to those in the real situation, which demonstrates the capacity of the estimation method.

Key words: Soil spatial variability; Probabilistic estimation; Displacement; Correlation length; Model test
https://doi.org/10.1631/jzus.A1900558 **CLC number:** TU4; P64

1 Introduction

The accurate estimation of soil parameters is required for feasible prediction of the performance of geotechnical structures. Site investigations with field tests and laboratory tests are common methods for estimating soil parameters. However, in situ soils exhibit natural spatial variability due to various factors (Phoon and Kulhawy, 1999a; Dasaka and Zhang, 2012; Crisp et al., 2019; Yang J et al., 2019a, 2019b). The soil parameters measured by field and laboratory tests may not be able to be used directly to predict soil behavior due to significant spatial variability (Novák et al., 2000; Li and Zhang, 2011; Yan et al., 2017; Phoon and Tang, 2019; Yang et al., 2020). For example, field measured soil parameters are influenced by the number and distribution of the drilling holes (Cao and Wang, 2013; Vardon et al., 2016; Jiang et al., 2018; Bilgin et al., 2019).

‡ Corresponding author
* Project supported by the National Natural Science Foundation of China (Nos. 51979158, 51639008, 51679135, and 51422905) and the Program of Shanghai Academic Research Leader (No. 19XD1421900), China
ORCID: Lu-lu ZHANG, https://orcid.org/0000-0001-8864-4377

In view of difficulties involved in direct estimation of soil parameters, various back analysis methods have been proposed for their estimation (Zhang SR et al., 2016; Zhang et al. 2017; Xiao et al. 2019; Sun et al., 2020). Ledesma et al. (1996) presented a probabilistic parameter estimation method based on the maximum likelihood approach. Gilbert et al. (1998) performed probabilistic back analyses for soil shear strength parameters based on a Bayesian updating method. Chowdhury et al. (2004) applied the Bayesian method to a slope failure to update the shear strength parameters and the probability of failure. Gavin and Xue (2009) proposed a back analysis method based on genetic algorithm (GA) to analyze the stability of unsaturated soil slopes. Wang et al. (2013) presented a probabilistic back analysis for estimating the friction angle and anchor forces for a landslide, and used the obtained parameters to update the probability of failure for the slope. Chao and Wang (2011) proposed a weighted back analysis method to consider the characteristics of displacement in different regions of a slope, i.e. the slip surface, slip mass, and slip bed. Zhang LL et al. (2010) proposed a probabilistic back analysis method based on Bayesian theory and Markov chain Monte Carlo (MCMC) simulation method. Zhang J et al. (2010) presented two methods for probabilistic back analysis of slope failure. One is based on an optimization approach and the other on a sensitivity analysis approach. Other studies focused on the identification of soil constitutive models (Jin et al., 2019a, 2019b, 2019c). Jin et al. (2019a) presented an enhanced version of the differential evolution-transitional MCMC (DE-TMCMC) method and a competitive Bayesian parameter identification approach for advanced soil models. Back analysis methods based on improved GAs were also proposed for the estimation of soil parameters (Jin et al., 2016, 2017, 2018; Yin et al., 2017). Mavritsakis (2017) conducted a comprehensive study of displacement inverse analysis considering spatial variability. The MCMC, GA, and regularized particle filter (RPF) methods were applied to displacement inverse analysis of an excavation. Young's modulus and the undrained shear strength of the soil were back estimated based on the horizontal displacements. The results showed that the GA was the most competent inverse analysis approach.

Some studies focused on the estimation of hydraulic properties. Chen and Zhang (2006) proposed a back analysis method based on the ensemble Kalman filter (EnKF) approach for continuously updating hydraulic conductivity and the pressure head through assimilating dynamic and static measurements. Zhang et al. (2013, 2014) proposed a probabilistic estimation method within a Bayesian framework and an MCMC simulation to estimate soil hydraulic parameters using field measured temporal pore water pressure data for a natural terrain slope in Hong Kong, China. Vardon et al. (2016) presented a method based on EnKF using pore pressure measurements to estimate the spatial variability of the hydraulic conductivity and constrain the uncertainty in the strength parameters using the cross-correlation of parameters. Liu et al. (2018) presented a data assimilation framework to sequentially improve the back estimation of spatially varied hydraulic parameters.

Few studies have been conducted to back estimate the spatial variability of soil parameters based on displacement measurements. In this study, the probabilistic estimation method proposed by Yang et al. (2018) was applied to characterize the spatial variability of soil parameters based on displacement responses. A numerical example is first presented to demonstrate the effects of the covariance function, variance, and correlation lengths on a slope with spatially varied elastic moduli. A second example is an application to laboratory model tests to investigate the capability of the method for use on stratified ground.

2 Probabilistic estimation method for spatial variability based on performance responses

2.1 Mathematical formulations of probabilistic estimation within a Bayesian framework

Numerical models are widely adopted to obtain the responses of displacement in geotechnical engineering (Ishii et al., 2012; Lee and Chang, 2012; Chen et al., 2013; Leshchinsky and Ling, 2013). In this study, numerical models were established using the finite element software ABAQUS and used as prediction models of soil responses.

The input parameters of the prediction model are an n-dimensional random vector $\boldsymbol{\theta}=\{\theta_1, \theta_2, \ldots, \theta_n\}$. The field measurement data and responses of the

prediction model at d monitoring points are represented by the vectors $\hat{\boldsymbol{P}}=\left\{\hat{P}_1,\hat{P}_2,...,\hat{P}_d\right\}$ and $\boldsymbol{P}(\boldsymbol{\theta})=\{P_1(\boldsymbol{\theta}),P_2(\boldsymbol{\theta}),...,P_d(\boldsymbol{\theta})\}$, respectively. $\hat{P}_i$ is the actual measurement and $P_i(\boldsymbol{\theta})$ is the predicted response of the model at the ith monitoring point (i=1, 2, …, d). The residual error between $\hat{\boldsymbol{P}}$ and $\boldsymbol{P}(\boldsymbol{\theta})$ is $\varepsilon=\{\varepsilon_1,\varepsilon_2,\ldots,\varepsilon_d\}$ with

$$\varepsilon_i(\boldsymbol{\theta}\mid\hat{\boldsymbol{P}})=P_i(\boldsymbol{\theta})-\hat{P}_i. \tag{1}$$

The residual errors are assumed to be mutually independent and Gaussian-distributed, thus the likelihood function can be expressed as (Box and Tiao, 2011; Yang et al., 2019c):

$$l(\boldsymbol{\theta}\mid\hat{\boldsymbol{P}})=\prod_{i=1}^{d}\frac{1}{\sqrt{2\pi\sigma_\varepsilon^2}}\exp\left(-\frac{(P_i(\boldsymbol{\theta})-\hat{P}_i)^2}{2\sigma_\varepsilon^2}\right), \tag{2}$$

where σ_ε^2 is the variance of the residual error.

Based on Bayesian theory (Tang and Ang, 2007), the posterior distribution of $\boldsymbol{\theta}$ is expressed as

$$h(\boldsymbol{\theta}\mid\hat{\boldsymbol{P}})=K\cdot l(\boldsymbol{\theta}\mid\hat{\boldsymbol{P}})\cdot h(\boldsymbol{\theta}), \tag{3}$$

where $h(\boldsymbol{\theta})$ is the prior distribution of $\boldsymbol{\theta}$, and K is a normalizing constant which can be expressed as

$$K=\left(\int l(\boldsymbol{\theta}\mid\hat{\boldsymbol{P}})\cdot h(\boldsymbol{\theta})\mathrm{d}\boldsymbol{\theta}\right)^{-1}. \tag{4}$$

An approach to characterize the spatial variability of soil parameters is to discretize the soil domain into numerous cells, the soil parameters of which are represented by the random vector $\boldsymbol{\theta}$. However, as the dimensionality of the random vector $\boldsymbol{\theta}$ may be prohibitively high, the probabilistic estimation of spatially varied soil parameters using Eq. (3) would be computationally intractable.

2.2 Efficient probabilistic characterization of spatial variability

To tackle this problem, Yang et al. (2018) presented an efficient probabilistic back estimation method to characterize the spatial variability of hydraulic properties. The method integrates the Karhunen-Loève (K-L) expansion, the polynomial chaos expansion (PCE), and the MCMC methods to estimate the spatial variability with high efficiency. In the following paragraphs, this method will be briefly introduced.

Firstly, the K-L expansion method (Karhunen, 1947; Loève, 1948) is used to discretize the random field of the spatially varied soil parameters. Consider a spatial domain $\boldsymbol{D}$, in which $\boldsymbol{x}$ is the spatial coordinate in $\boldsymbol{D}$. The spatially varied soil properties (e.g. elastic modulus E) are characterized by a spatial random variable $E(\boldsymbol{x})$ with mean $\mu(\boldsymbol{x})$ and covariance function $C(\boldsymbol{x}_1,\boldsymbol{x}_2)$. $C(\boldsymbol{x}_1,\boldsymbol{x}_2)$ is symmetric and positive finite and can be expressed as (Huang et al., 2001):

$$C(\boldsymbol{x}_1,\boldsymbol{x}_2)=\sum_{i=1}^{\infty}\lambda_i\varphi_i(\boldsymbol{x}_1)\varphi_i(\boldsymbol{x}_2), \tag{5}$$

where $\varphi_i(\boldsymbol{x})$ and λ_i are the eigenvectors and eigenvalues of $C(\boldsymbol{x}_1,\boldsymbol{x}_2)$, respectively. The method for calculating $\varphi_i(\boldsymbol{x})$ and λ_i can be found in (Atkinson, 1967). The K-L expansion of $E(\boldsymbol{x})$ can be expressed as (Ghanem and Spanos, 2003):

$$E(\boldsymbol{x})=\mu(\boldsymbol{x})+\sum_{i=1}^{\infty}\sqrt{\lambda_i}\xi_i\varphi_i(\boldsymbol{x}), \tag{6}$$

where ξ_i is the ith independent standard normal random variable. These Gaussian random variables reflect the uncertainty of eigenvectors only on the generated spatial field of $E(\boldsymbol{x})$.

In practical application, the K-L expansion is often truncated for the desired accuracy. Commonly, the truncation level m is determined such that 95% of the total variability is preserved (Jiang et al., 2015):

$$\frac{\sum_{i=1}^{m}\lambda_i}{\sum_{i=1}^{\infty}\lambda_i}=0.95. \tag{7}$$

In this study, the basic random vector $\boldsymbol{\xi}$ is used as the input parameter vector $\boldsymbol{\theta}$ of the prediction model instead of the spatial random variable $E(\boldsymbol{x})$. Hence, the high dimensional random vector $E(\boldsymbol{x})$ can be

represented with the random vector $\boldsymbol{\xi}=\{\xi_1, \xi_2, \ldots, \xi_m\}$ with low dimensionality as

$$E(\boldsymbol{x}) = \mu(\boldsymbol{x}) + \sum_{i=1}^{m} \sqrt{\lambda_i}\,\xi_i \varphi_i(\boldsymbol{x}). \tag{8}$$

To further improve computational efficiency, a surrogate model based on the PCE method is established to substitute for the original prediction model. The response of the original prediction model $P(\boldsymbol{\xi})$ can be approximated by the surrogate model $P_s(\boldsymbol{\xi})$ as (Ghanem and Spanos, 1991; Pan et al., 2020):

$$P(\boldsymbol{\xi}) \approx P_s(\boldsymbol{\xi}) = \sum_{j=0}^{k-1} c_j \Psi_j(\boldsymbol{\xi}), \tag{9}$$

where k is the number of multi-dimensional orthogonal polynomials $\Psi_j(\boldsymbol{\xi})$, and c_j are the unknown coefficients. In this study, the basic random vector $\boldsymbol{\xi}$ from the K-L expansion is Gaussian. Hence, Hermite polynomials are adopted for orthogonal polynomials $\Psi_j(\boldsymbol{\xi})$. To calculate the unknown coefficients c_j, the projection method with sparse grid collocation based on the Smolyak algorithm is adopted for high efficiency and accuracy (Smolyak, 1963; Xiu, 2007).

Finally, the posterior distribution of $\boldsymbol{\xi}$ can be expressed as

$$h(\boldsymbol{\xi} \mid \hat{\boldsymbol{P}}) = K \cdot \prod_{i=1}^{d} \frac{1}{\sqrt{2\pi\sigma_\varepsilon^2}} \exp\left(-\frac{(P_{si}(\boldsymbol{\xi}) - \hat{P}_i)^2}{2\sigma_\varepsilon^2} \right) \cdot h(\boldsymbol{\xi}). \tag{10}$$

As Eq. (10) is difficult to solve using analytical methods, an adaptive MCMC method entitled the differential evolution adaptive metropolis (DREAM) algorithm (Vrugt et al., 2008) is adopted to solve it. The convergence of the DREAM algorithm can be calculated using the R criterion of Gelman and Rubin (1992). The convergence diagnostic R_{stat} value is required to be less than 1.2 to declare convergence to a stationary distribution. Details of the algorithm can be found in (Vrugt et al., 2008). When the posterior estimation of $\boldsymbol{\xi}$ is obtained, the K-L expansion is used to construct the estimated random field using Eq. (8).

3 Numerical example: a soil slope subject to a surcharge load

3.1 Stochastic finite element model and soil parameters

A numerical model of a soil slope subject to a surcharge load was established based on the finite element software ABAQUS. The slope was inclined at 40° and was 20 m high. The vertical boundaries (*AB*, *CD*) were constrained in the horizontal direction. The bottom boundary (*BC*) was constrained in both the horizontal and vertical directions. A surcharge load, q=10 kPa, was applied to the top (*AF*) of the slope. The purpose of the surcharge load was to simulate the load from construction vehicles, filled materials or low-rise buildings on the top of the slope which may cause displacement of the slope. Note that the focus of this study was on the back estimation of the spatial variability using displacements. The surcharge load was not supposed to induce slope failure. The geometry and finite element mesh of the soil slope are illustrated in Fig. 1. There were 288 nodes and 272 elements in the finite element model. The input parameters of the slope are summarized in Table 1. The soil in the slope was assumed to be sandy, with a density of 1800 kg/m³.

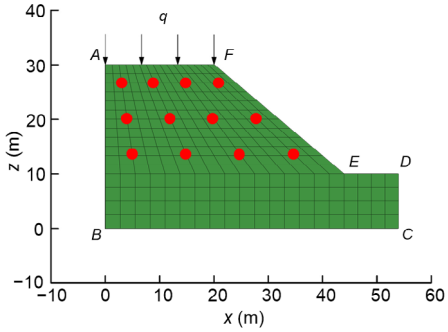

Fig. 1 Illustration of geometry and finite element mesh of the soil slope

Table 1 Input parameters of the numerical example

Parameter	Value
Density, ρ (kg/m³)	1800
Mean of E, μ_E (MPa)	10
Standard deviation of E, σ_E (MPa)	1
Poisson's ratio, λ	0.3
Surcharge load, q (kPa)	10
Correlation length in horizontal direction, l_h (m)	50
Correlation length in vertical direction, l_v (m)	10

To evaluate the effects of mesh density on the displacement responses, three models with different finite element mesh densities (Fig. 2) were compared. The models with small, medium, and large mesh densities were meshed into 68, 272, and 1088 elements, respectively. Table 2 compares the horizontal displacements of the 12 monitoring points of the slope with different mesh densities. The variation in displacements with different mesh densities was extremely small. The maximum horizontal displacements for the models with the small, medium, and large mesh density were 0.461, 0.462, and 0.463 cm, respectively. Hence, the mesh density had little effect on displacement responses. As the back estimation of spatial variability is based on the displacement responses, the mesh density had little effect on the back estimation. The mesh density in the study met the requirement for accuracy.

Table 2 Comparison of the horizontal displacements of the 12 monitoring points with different mesh densities

Monitoring point	Horizontal displacement (cm)		
	Small mesh density	Medium mesh density	Large mesh density
1	0.114	0.113	0.114
2	0.339	0.338	0.338
3	0.434	0.434	0.433
4	0.383	0.384	0.384
5	0.071	0.071	0.071
6	0.247	0.248	0.249
7	0.415	0.416	0.416
8	0.447	0.448	0.448
9	0.001	0.002	0.002
10	0.018	0.016	0.016
11	0.081	0.078	0.079
12	0.183	0.185	0.185

The elastic modulus E is closely related to the displacement responses of a slope and has a significant variability in space. In the example, E was assumed to be a spatially random variable. As the numerical example was not used to investigate the stability of the slope, but to obtain the displacement for back estimation, the soil was assumed to be an elastic model without considering the plasticity of the material. According to Bowles (1996), the elastic modulus of loose sands ranges from 10 to 25 MPa and Poisson's ratio λ of sandy soils ranges from 0.3 to 0.4. In the example, Poisson's ratio λ was 0.3. In geotechnical engineering, soil parameters such as E and shear strength are positive, and can be characterized by a log-normal distribution (Fenton and Griffiths, 2002; Baecher and Christian, 2003; Jiang et al., 2014; Li et al., 2014; Qi and Li, 2018; Yang et al., 2018).

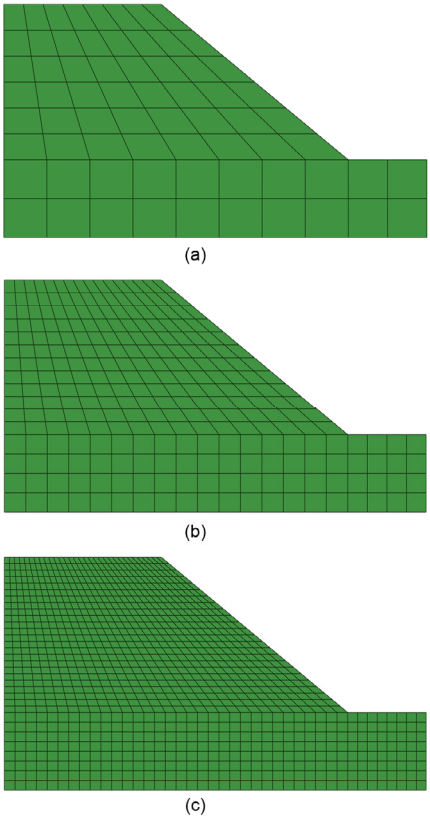

Fig. 2 Soil slope with different finite element mesh densities: (a) small mesh density; (b) medium mesh density; (c) large mesh density

In the example, E was assumed to follow a log-normal distribution and the mean μ_E and coefficient of variation COV_E were assumed to be 10 MPa and 0.1, respectively. The spatial variability of ln$E$ was characterized by a statistically stationary random field with the Gaussian covariance function:

$$C(\boldsymbol{x}_1,\boldsymbol{x}_2)=\sigma^2\exp\left\{-\pi\left[\frac{(x_1-x_2)^2}{\delta_{\mathrm{h}}^2}+\frac{(z_1-z_2)^2}{\delta_{\mathrm{v}}^2}\right]\right\}, \quad (11)$$

where (x_1, z_1) and (x_2, z_2) are the coordinates of two points in space; σ^2 is the variance of ln$E$; δ_{h} and δ_{v} are the scales of fluctuation in the horizontal and vertical directions, respectively. Here, the scale of fluctuation can be substituted by another scaling coefficient, i.e. correlation length. The Gaussian covariance function

can then be expressed as

$$C(\boldsymbol{x}_1,\boldsymbol{x}_2)=\sigma^2\exp\left\{-\left[\frac{(x_1-x_2)^2}{l_{\mathrm{h}}^2}+\frac{(z_1-z_2)^2}{l_{\mathrm{v}}^2}\right]\right\}, \quad (12)$$

where l_{h} and l_{v} are the coefficients in the horizontal and vertical directions with $\delta_{\mathrm{h}}=\sqrt{\pi}l_{\mathrm{h}}$ and $\delta_{\mathrm{v}}=\sqrt{\pi}l_{\mathrm{v}}$, respectively. According to the literature (Phoon and Kulhawy, 1999a; Li DQ et al., 2015; Li JH et al., 2016; Zhang LL et al., 2016), the horizontal scale of fluctuation is generally larger than 10 m and can sometimes approach 100 m. In contrast, the vertical scale of fluctuation is generally less than 10 m. Fig. 3 shows the effect of l_{v} on the sum of the K-L eigenvalues λ_i for the exponential covariance function. The number of terms of the K-L expansion required to approximate $\ln E(\boldsymbol{x})$ increases with the reduction of l_{v}. As a base case in this example, l_{h} and l_{v} were firstly assumed to be 50 m and 10 m, respectively. The truncation level was taken as 5 so that 95% of the total variability of the random field could be preserved. The random field of $\ln E$ can be expressed as

$$\ln\hat{E}(\boldsymbol{x})=\mu_{\ln E}+\sigma_{\ln E}\left(\sum_{i=1}^{5}\sqrt{\lambda_i}\xi_i\varphi_i(\boldsymbol{x})\right), \quad (13)$$

where $\ln\hat{E}(\boldsymbol{x})$ is the approximation of $\ln E(\boldsymbol{x})$ and is represented by five basic random variables ξ_i (i=1, 2, …, 5); $\mu_{\ln E}$ and $\sigma_{\ln E}$ are the mean and standard deviation, respectively, of $\ln E$ and can be expressed as

$$\begin{aligned}\sigma_{\ln E}&=\sqrt{\ln(1+(\sigma_E/\mu_E)^2}\,,\\ \mu_{\ln E}&=\ln\mu_E-0.5\sigma_{\ln E}^2.\end{aligned} \quad (14)$$

Hence, the random field of $\hat{E}(\boldsymbol{x})$ can be expressed as

$$\hat{E}(\boldsymbol{x})=\exp\left(\mu_{\ln E}+\sigma_{\ln E}\left(\sum_{i=1}^{5}\sqrt{\lambda_i}\xi_i\varphi_i(\boldsymbol{x})\right)\right). \quad (15)$$

The five basic random variables from the truncated K-L expansion were estimated using the probabilistic estimation method. The whole domain was 53.85 m×30 m and was discretized into 20×16=320 cells. As the number of random variables to be estimated was much smaller than the number of cells, the dimensionality of parameter estimation was significantly reduced. Note that for other random fields in the following sections, the truncation level and the number of basic random variables will be determined correspondingly, based on the specific spatial parameters, to preserve 95% of the total variability.

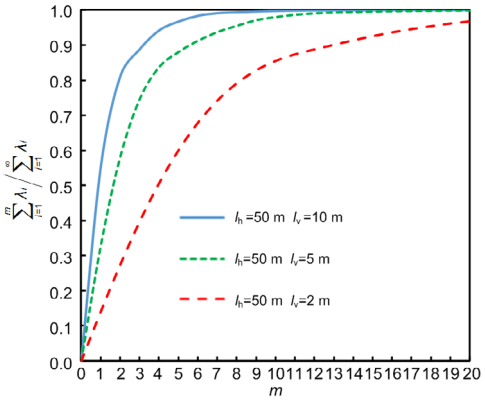

Fig. 3 Sum of the K-L eigenvalues λ_i with different vertical correlation lengths

3.2 Construction of surrogate model

In practical application, the degree of PCE ranges from 1 to 7 (Huang et al., 2007; Jiang et al., 2014). When the degree increases, the accuracy of the surrogate model is efficiently improved, but the computational load increases significantly. In this example, the degree p=2 of PCE was chosen so that the computational cost was relatively small and the accuracy of PCE was also acceptable, as shown below.

According to Ghanem and Spanos (1991), the number of the unknown coefficients of the surrogate model is $\frac{(2+5)!}{2!\times 5!}=21$. To calculate the unknown coefficients, 81 sets of collocation points of the basic random vector $\boldsymbol{\xi}$ were selected using the sparse grid collocation method. For each set of collocation points, a random field of E was generated using the K-L expansion method. A monitoring system with 12 measurement points was set in the slope (Fig. 1). Usually, horizontal displacements are measured using inclinometers or rod extensometers, and vertical deformations are measured by settlement cells. The displacement responses at these measurement points for each generated random field were obtained using

the finite element model. The unknown coefficients c_j of the surrogate model $P_s(\boldsymbol{\xi})$ in Eq. (9) were then calculated using the projection method based on the displacement responses. The surrogate models for both vertical and horizontal displacements at the 12 measurement locations in the slope were established.

To verify the accuracy of the surrogate models, 200 random samples of the basic random vector $\boldsymbol{\xi}$ were generated from the Gaussian distribution and used to obtain the displacement responses according to the surrogate model $P_s(\boldsymbol{\xi})$. The correlation coefficient r and root mean square error (RMSE) were used to measure the differences between the displacements of the original finite element model $P(\boldsymbol{\xi})$ and the surrogate model $P_s(\boldsymbol{\xi})$. The r values for the horizontal and vertical displacements were both 1.000. The RMSE values of the horizontal and vertical displacements were 0.0012 mm and 0.0046 mm, respectively. Hence, the responses of the surrogate model and the original model were almost identical, indicating that the PCE surrogate model can efficiently substitute for the finite element model of slope stability analysis.

4 Probabilistic estimation

A hypothetical field with COV_E=0.1, l_h=50 m, and l_v=10 m was randomly generated. This field was taken as the true field and could be characterized by the first five eigenfunctions to preserve 95% of the total variability. Hence, these first five Gaussian random variables were regarded as the true values and were estimated. According to Ahmed et al. (2015), generally 1%–5% random fluctuations are added into the responses to generate artificial data. If the noise is too large, the accuracy of estimation may be affected. In contrast, if the noise is too small, the effect of measurement errors and model errors may not be considered effectively. In the example, the displacement responses obtained from the finite element model were corrupted with 2% Gaussian noise. The spatial variability of E was then estimated based on these artificial data.

4.1 Posterior distribution of basic random variables

A total of 10 Markov chains with 100 000 samples were used in the MCMC simulation. The model output is log-likelihood. As the random variables in the K-L expansion are independent Gaussian random variables, the prior distribution of each random variable is a standard normal distribution and the five random variables are independent. In the DREAM algorithm, there is no upper or lower limit on the values of all random variables. There were three crossover values and three chain pairs. The random error for ergodicity was 0.05, and the probability of a jump rate of 1 was 0.2. The scaling factor of the built-in jump rate was 1. The result shows that 5000 samples were enough to declare convergence of each random variable to a stationary posterior distribution. The MCMC simulation for 5000 samples took only about 1 min, indicating that the computational cost of probabilistic estimation based on the surrogate model was negligible.

The last 25% of samples of the 10 Markov chains were used as stationary samples from the posterior distributions. Fig. 4 shows the posterior distributions of the five random variables based on horizontal and vertical displacements. The posterior distributions were well identified within a very small region. For each random variable, the posterior distribution based on horizontal displacements was narrower than that based on vertical displacements. The posterior mean and standard deviation of the random variables are summarized in Table 3. For the five random variables, the posterior means of ξ_2 and ξ_3 based on horizontal and vertical displacements were almost the same. The maximum relative error between the posterior mean based on horizontal and vertical displacements was only 1.2% (ξ_4). Thus, the posterior mean of the five random variables based on horizontal and vertical displacements were close to each other. The maximum posterior standard deviation of the five random variables based on horizontal and vertical displacements were 0.0037 and 0.0066, respectively. Hence, the uncertainties of the random variables were significantly reduced. The standard deviation based on horizontal displacements was less than that based on vertical displacements. Thus, the uncertainty reduction based on horizontal displacements was less than that based on vertical displacements.

In this study, the optimal value of each random variable was represented by the maximum posterior density (MPD) value. A comparison between the true

value and optimal value of the random variables is illustrated in Table 4. The maximum relative errors based on horizontal and vertical displacements were only 0.76% (ξ_3) and 1.04% (ξ_4), respectively. Thus, the optimal values based on horizontal and vertical displacements were both close to the true value for each random variable, indicating that the random variables can be estimated with high accuracy.

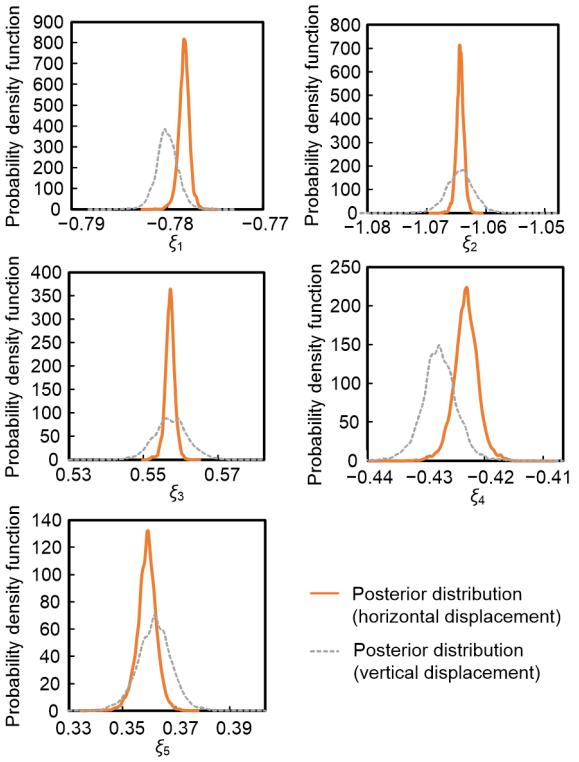

Fig. 4 Posterior distributions of the five random variables based on horizontal and vertical displacements

4.2 Estimation of spatial variability

The estimated field of E was obtained based on the optimal value of the random variables. Figs. 5a and 5b show the relative error of the estimated field (COV_E=0.1, l_h=50 m, and l_v=10 m) based on horizontal and vertical displacements, respectively. The maximum relative errors based on horizontal and vertical displacements were 0.02% and 0.04%, respectively. Thus, the estimated field was extremely close to the true field. Note that the maximum relative error of the estimated field based on horizontal displacements was smaller than that based on vertical

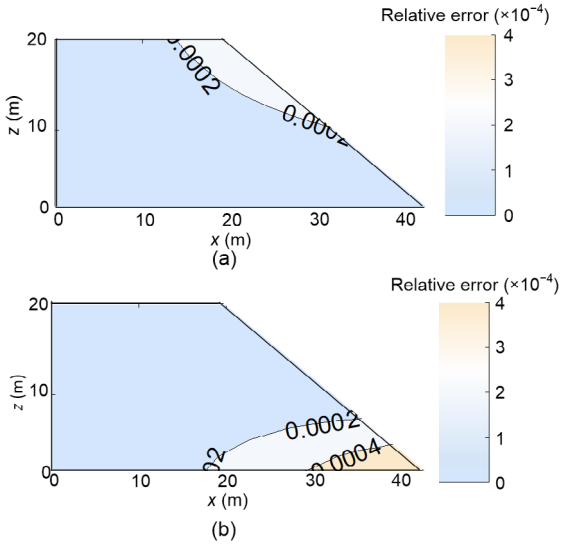

Fig. 5 Relative errors of the estimated field (l_h=50 m, l_v=10 m, COV_E=0.1) based on horizontal displacements (a) and vertical displacements (b)

Table 3 Posterior mean and standard deviation of the random variables based on horizontal and vertical displacements for the true field in Fig. 6a

Statistics	ξ_1	ξ_2	ξ_3	ξ_4	ξ_5
True	−0.778	−1.064	0.553	−0.423	0.362
Mean (horizontal)	−0.778	−1.064	0.557	−0.423	0.359
Mean (vertical)	−0.780	−1.064	0.556	−0.428	0.362
Std. (horizontal)	5.78×10^{-4}	6.67×10^{-4}	0.0012	0.0021	0.0037
Std. (vertical)	0.0012	0.0024	0.0048	0.0032	0.0066

Table 4 Comparison between the optimal and true values of the random variables for the true field in Fig. 6a

Statistics	ξ_1	ξ_2	ξ_3	ξ_4	ξ_5
True	−0.778	−1.064	0.553	−0.423	0.362
Optimal (horizontal)	−0.778	−1.064	0.557	−0.423	0.359
Optimal (vertical)	−0.780	−1.064	0.556	−0.428	0.362
Relative error (horizontal)	0.01%	0.08%	0.76%	0.09%	0.55%
Relative error (vertical)	0.27%	0.04%	0.52%	1.04%	0.03%

displacements. Hence, the estimation based on horizontal displacements was more accurate, and horizontal displacements are preferred for displacement back estimation of the spatial variability of E.

5 Effects of spatial structure on estimation

The spatial structure of E affected the truncation level of the K-L expansion (Fig. 3). This may influence the accuracy of probabilistic estimation. In this section, the effects of the covariance function, COV_E, and correlation lengths on the estimation of spatial variability are investigated. As shown in the previous section, the estimation based on horizontal displacements is more accurate. Thus, only the horizontal displacements are considered in this section.

5.1 Effect of uncertainty level

A pressure meter test (PMT) provides a direct measurement of the horizontal modulus of soils. This modulus (E_{PMT}) often is presumed to be roughly equivalent to E, and the coefficient of variation (COV) of E_{PMT} is generally not more than 0.95 (Phoon and Kulhawy, 1999b). Figs. 6a, 6d, 6g, and 6j show three true fields with different values of COV_E (0.1, 0.5, 0.9, and 1.5, respectively), to represent typical fields with weak, median, strong, and very strong variability. For all four fields, l_{h}=50 m and l_{v}=10 m. The corresponding estimated fields and

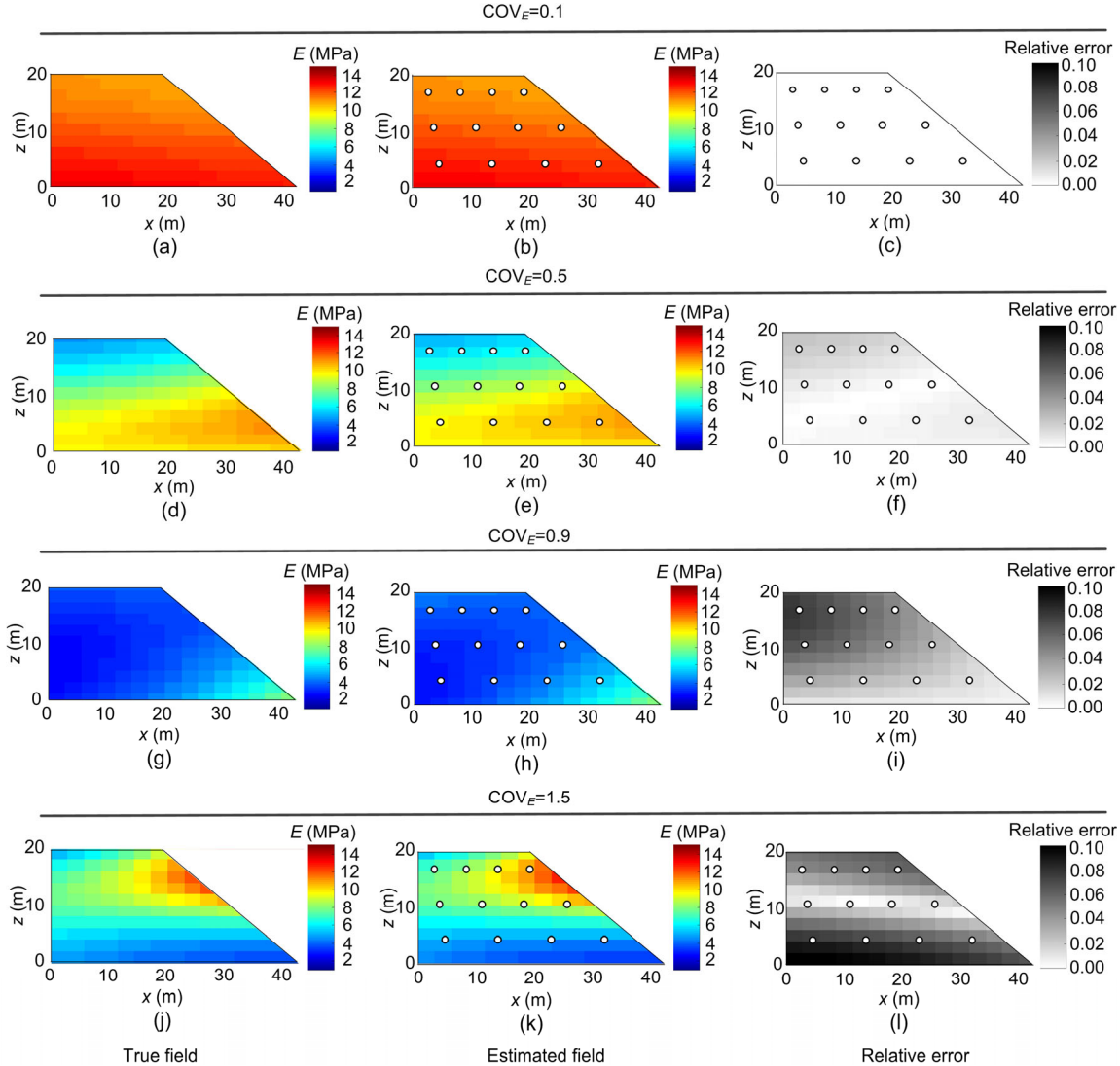

Fig. 6 True fields, estimated fields, and relative errors for COV_E=0.1 (a)–(c), 0.5 (d)–(f), 0.9 (g)–(i), and 1.5 (j)–(l)

absolute relative errors are also presented in Fig. 6. As variability increased, the accuracy of estimation reduced greatly. The maximum absolute relative error was less than 0.1% (0.02%) when the COV_E was 0.1. This result indicates that when the spatial variability of E is weak, the spatially varied elastic moduli can be estimated with high accuracy. When the COV_E increased to 0.5, the corresponding error was about 2.5%. The error increased to 8% when the COV_E was 0.9, and to about 10% when the COV_E increased to 1.5. Hence, the accuracy of back estimation is generally acceptable although the spatial variability is very strong.

Fig. 7 shows a comparison of calculated displacements between the numerical model and surrogate model for a spatially varied slope with different COV_E values. Points on the graph with different colors characterize different locations on the slope (please refer to the web version). The RMSE increased and the correlation coefficient r decreased with the increase of the COV_E. Hence, the accuracy of the surrogate model is reduced as the COV_E increases.

When the COV_E was 0.9, the maximum horizontal displacement was 30.50 mm and the RMSE was 0.6707 mm. The RMSE was about 2.2% of the maximum horizontal displacement. For some points of small displacements, the error between displacements of the finite element model and surrogate model was relatively large (Fig. 7c). The nonlinearity of the model due to spatial variability was strong when the variability was large. Hence, this discrepancy between the original model and the surrogate model contributed to the final estimation error.

For the true field shown in Fig. 6g, a series of estimated fields in addition to the MPD estimation (Fig. 6h) can be generated based on the stationary posterior samples. The corresponding displacement fields of these estimated fields were calculated with posterior samples. Fig. 8 shows the COV of the displacement fields for COV_E=0.9. The COVs of the upper left part of the area enclosed by the 12 points were relatively large. The maximum COV was close to 0.1. The relative errors of estimated fields were also relatively large in the upper left part of the same area (Fig. 6i). For the locations where the relative error of the estimated field was large, the COV of the predicted displacements was also large. Hence, the accuracy of back estimation can affect the uncertainty of predicted displacements.

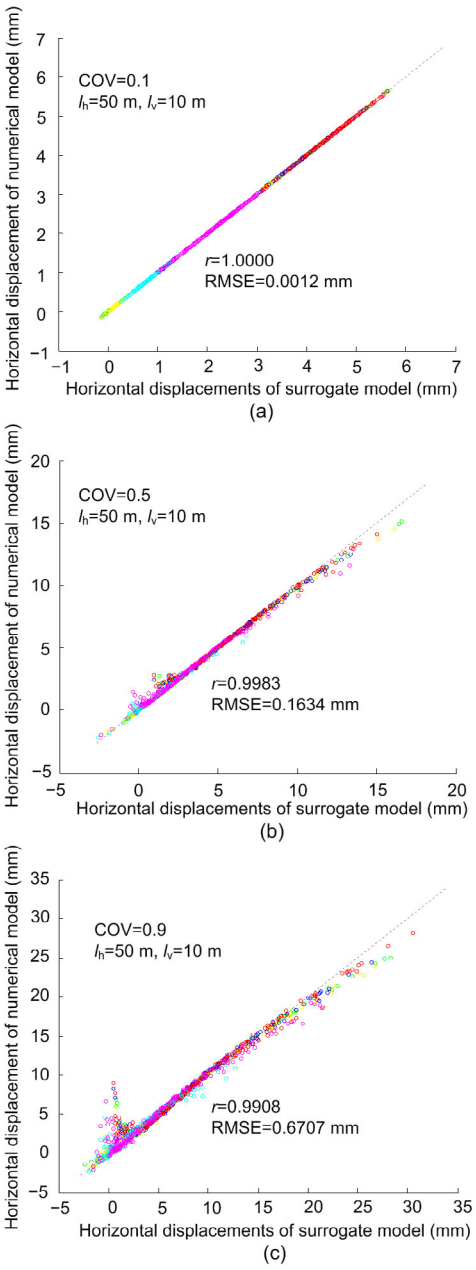

Fig. 7 Comparison of horizontal displacements between the original model and the surrogate model for a spatially varied slope with COV_E=0.1 (a), 0.5 (b), and 0.9 (c)

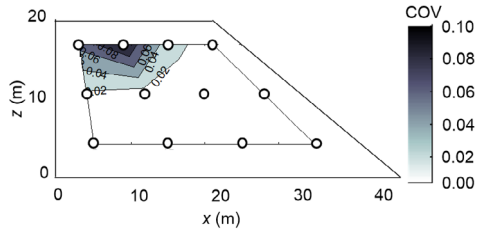

Fig. 8 COV of displacements based on stationary samples with COV_E=0.9, l_h=50 m, and l_v=10 m

5.2 Effect of covariance function

Spatially varied fields with different covariance functions were investigated. In this study, the second-order Markov covariance function (Li et al., 2015) was compared with the Gaussian covariance function (Eq. (11)). The second-order Markov covariance function is as follows:

$$C(\boldsymbol{x}_1,\boldsymbol{x}_2)=\sigma^2\exp\left[-4\left(\frac{|x_1-x_2|}{\delta_{\mathrm{h}}}+\frac{|z_1-z_2|}{\delta_{\mathrm{v}}}\right)\right]\times\left(1+\frac{4|x_1-x_2|}{\delta_{\mathrm{h}}}\right)\left(1+\frac{4|z_1-z_2|}{\delta_{\mathrm{v}}}\right). \tag{16}$$

For comparison, the scales of fluctuation of the Gaussian function and the second-order Markov covariance function were the same. The truncation level of the K-L expansion to conserve 95% total variability for the second-order Markov covariance function was 12. Fig. 9 shows the true fields, the estimated fields, and the errors generated with different covariance functions. When the second-order Markov covariance function was used, the maximum error was 1.2%. Hence, the accuracy of estimation is affected by the type of covariance function even when the total variability is small (COV_E=0.1).

Fig. 10 compares the maximum relative errors for the two covariance functions with different levels of variability. As shown in the graph, the accuracy of estimation was significantly affected by the covariance function. When the COV_E was 0.5, the maximum relative error with the second-order Markov covariance function was 8.5% whereas it is less than 3% for Gaussian covariance. This discrepancy probably occurred because the number of random variables can also affect the performance of probabilistic estimation. As the dimension of $\boldsymbol{\xi}$ in Eq. (10) was 12 for the spatially varied field with the second-order Markov covariance function, the capability of parameter estimation by MCMC was not efficient enough and therefore the relative error is large.

5.3 Effect of correlation lengths

Fig. 11 shows the true fields with different horizontal correlation lengths l_{h} (50, 25, and 15 m), the optimal estimated fields, and the error distributions.

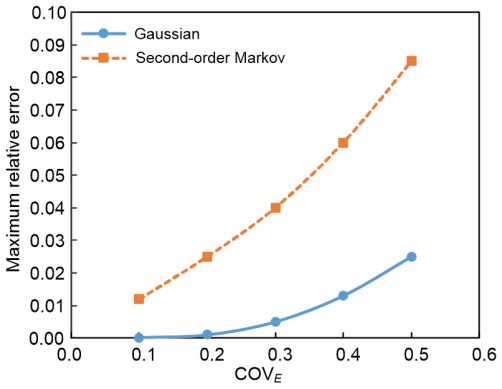

Fig. 10 Variation of the maximum relative error with COV_E

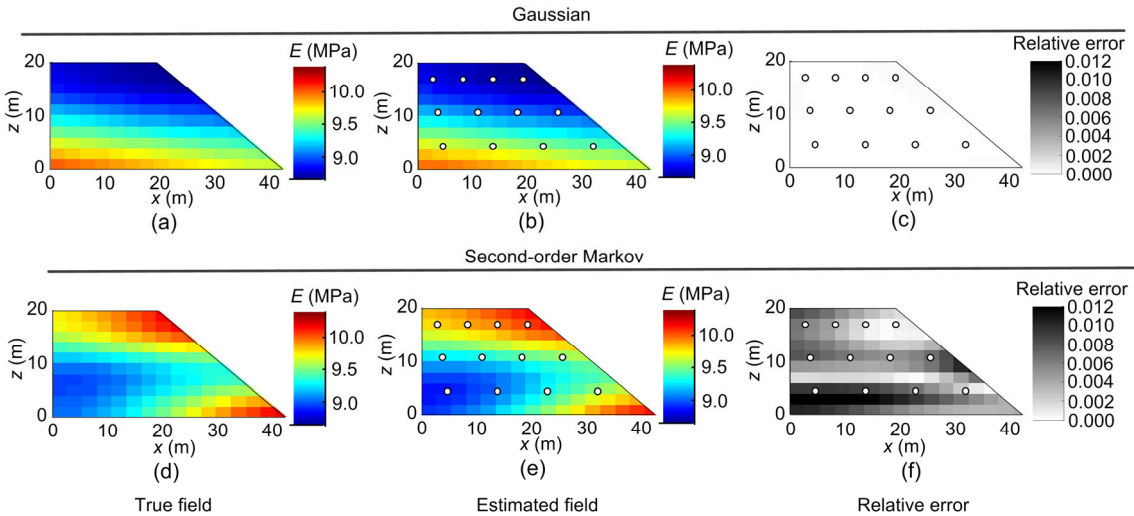

Fig. 9 True fields, estimated fields, and relative errors (COV_E=0.1, l_{h}=50 m, l_{v}=10 m) for Gaussian (a)–(c) and second-order Markov (d)–(f)

In the three cases, COV_E=0.1 and l_v=10 m. In general, the accuracy of estimation was reduced as l_h decreased. When l_h was reduced to 25 m, the maximum relative error was about 0.4%, and when l_h was 15 m, the maximum error was about 4%. These results show that when the correlation of E in the horizontal direction is relatively strong, the accuracy of the estimation is still acceptable.

Fig. 12 shows the effect of the vertical correlation length l_v on the estimated fields and relative errors. In the three cases, COV_E=0.1 and l_h=50 m. Comparing with Fig. 11, the results show that the accuracy of estimation is more affected by the vertical correlation length l_v. When l_v was reduced to 5 m, the maximum relative error was about 1%, and when l_v was further reduced to 2 m, the maximum error was up to 12%, indicating that the accuracy is relatively low when the spatial correlation along the vertical direction is strong.

6 Laboratory model tests

A series of laboratory model tests were conducted to demonstrate the application of the probabilistic estimation method to real situations. The setup of the model test is shown in Fig. 13a. The tests were conducted inside a model box made of acrylic plates and steel frames. The inner length, width, and height of the model box were 50, 25, and 36 cm, respectively. Two types of materials, i.e. gravel and plastic particles, were used to simulate a ground with layers of soils. A force was applied on a panel on the right side of the box causing deformation of the ground. Once the displacement of the right panel was up to 18 mm, the test was terminated.

The particle size of the gravel ranged from 2 to 4 mm with an average value of 3 mm. The plastic particles were made of polyethylene with an average particle size of 5 mm. The angles of repose of the dry gravel and plastic particles were measured to be about 30° and 22°, respectively. Hence, the internal friction angles ϕ of the soil layers were considered to be equal to the corresponding angles of repose. A 45 cm× 20 cm mesh of 171 (19×9) monitoring points with 2.5 cm spacing is shown in Fig. 13a. The displacements (Fig. 13b) of the model were obtained based on high resolution image analysis of the monitoring points using the particle image velocimetry (PIV) technique with PhotoInfor software (Li YH et al., 2016).

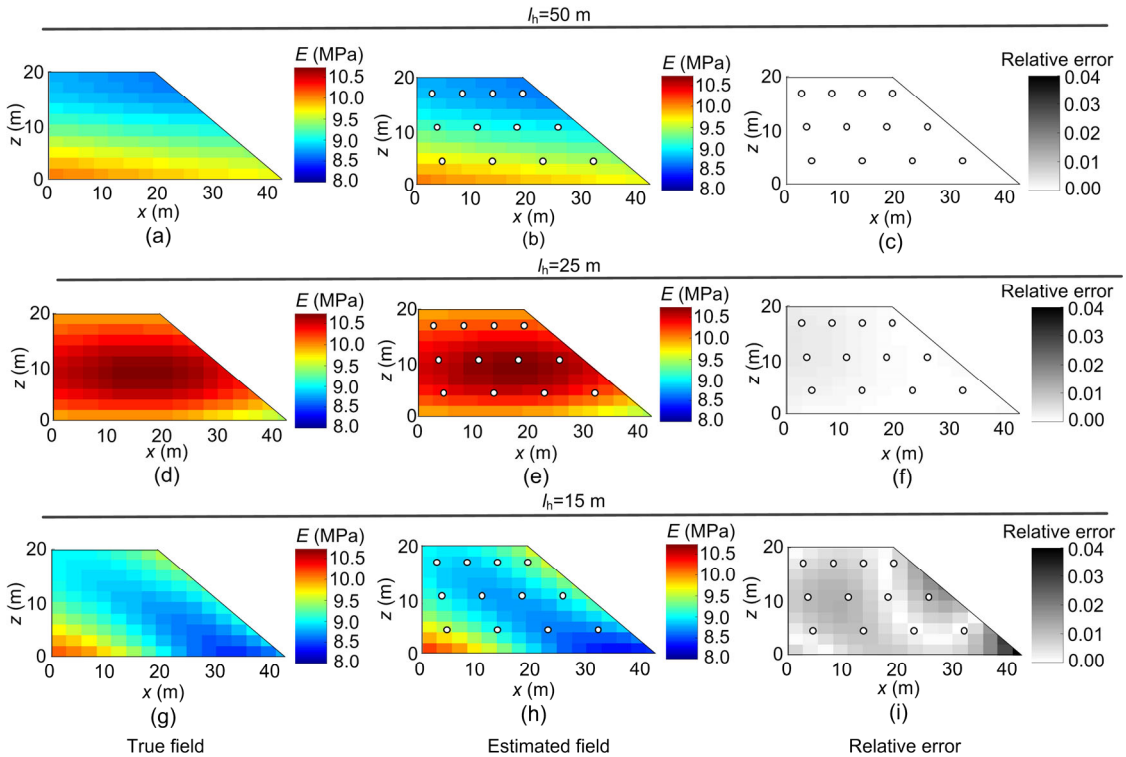

Fig. 11 True fields, estimated fields, and error distributions for l_h=50 m (a)–(c), 25 m (d)–(f), and 15 m (g)–(i)

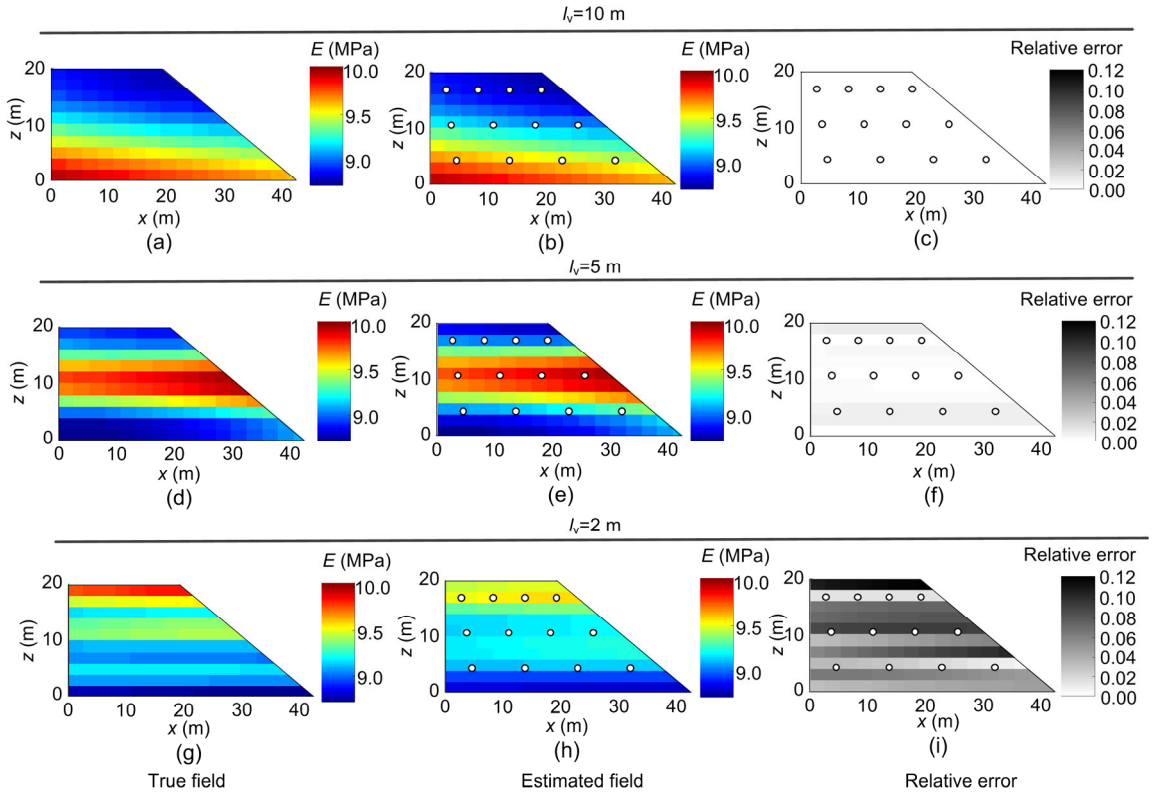

Fig. 12 True fields, estimated fields, and error distributions for l_v=10 m (a)–(c), 5 m (d)–(f), and 2 m (g)–(i)

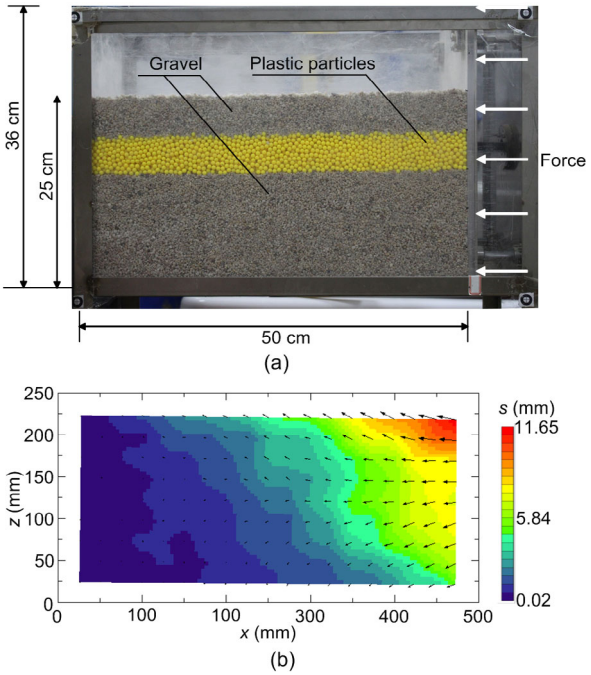

Fig. 13 Set up of the model test (a) and measured displacement *s* distribution of test 1 (b)

The soil layers of the three model tests are shown in Figs. 14a–14c. The plastic particle layers of tests 1, 2, and 3 were 5, 5, and 10 cm thick, respectively. The measured displacement s fields are shown in Figs. 14g–14i. The spatial variability of the model test is mainly in the vertical direction as layered ground. Thus, for probabilistic estimation, the horizontal correlation length was taken as 1 m, which is much larger than vertical correlation length of 0.05 m. The prior mean value and coefficient of variation of ϕ were taken as 25° and 0.3, respectively. The internal friction angles of the soil layers were back estimated based on the horizontal displacements.

As the random field model embedded in the probabilistic estimation method is a continuous model, the soil layers in the ground cannot be distinctly separated. However, the soil layers can be roughly identified with transition zones (Figs. 14d–14f). The estimated ϕ of gravel generally ranges from 28° to 29° and the estimated ϕ of plastic particles ranges from 22° to 24°. The estimation error was less than 10%.

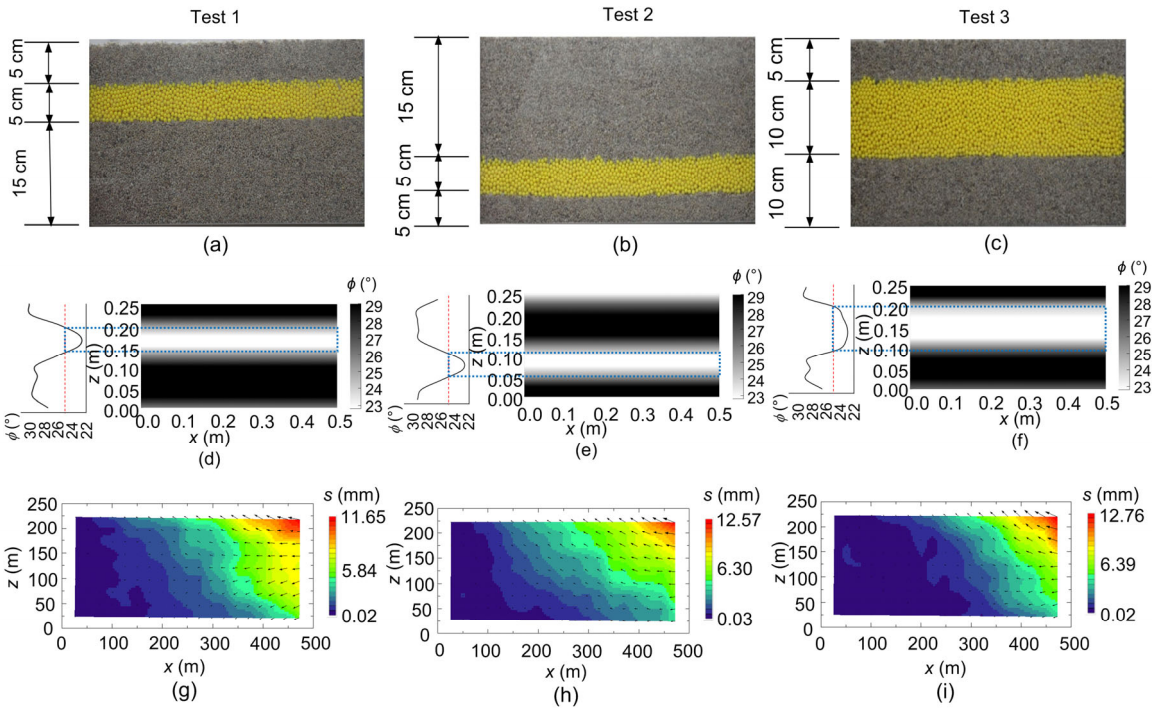

Fig. 14 Soil layers in the domain (a)–(c), the estimated field of ϕ (d)–(f), and the measured displacement s field (g)–(i) of tests 1, 2, and 3

Assume 25° is the threshold value of the friction angle to differentiate the two layers. The estimated thicknesses of the plastic particle layer were about 7, 8, and 11 cm for the three model tests, respectively, which is only slightly different from the actual situation. Comparing Figs. 14d–14f, it can also be found that the location and thickness of the plastic particle layer had no significant effect on the estimation.

7 Conclusions

In this paper, a probabilistic estimation method of spatial variability was applied to displacement back estimation of a hypothetical soil slope example and a verification example of model tests. The major conclusions are summarized below:

1. For the base case, the maximum relative errors based on horizontal and vertical displacements were only 0.02% and 0.04%, respectively. The use of horizontal displacement is preferable to the use of vertical displacement for back estimation.

2. The accuracy of estimation is affected by the type of covariance function and the variance. However, the estimation is generally acceptable, as the error is not more than 10%, even for the high variance case (COV_E=1.5). When the correlation length decreases, the accuracy of estimation is reduced.

3. For the verification example of model tests, the soil layers in the artificial ground could be identified and the estimation error of the friction angle was less than 10%. Assuming the threshold value of the friction angle between the two materials was 25°, the estimated thicknesses of the plastic particle layer were 7, 8, and 11 cm, respectively, for the three model tests, which is only slightly different from the actual situation.

In this study, only one soil property was estimated using the probabilistic back estimation method of spatial variability. However, multiple soil properties can influence soil behavior at the same time. For example, the elastic modulus, shear strength, and soil density of a sandy soil can all affect the mechanical behavior of a geotechnical structure. The present method could be further extended to estimate the spatial variability with multiple random variables.

In the model tests, the ground was formed of

several distinct soil layers to represent spatial variability due to interlayer heterogeneity. The present method is able to capture spatial variation, but the fields should be Gaussian random fields. Hence, the distinct boundaries between soil layers cannot be described. To simplify the problem, only the stratification was verified with the actual situations in tests. To extend the present method to ground conditions with distinct layer interfaces, such as geological anomalies and facies, other random field simulation methods such as sequential indicator simulation should be used to describe the spatial field. Further studies should be conducted to extend the present method to situations with different types of heterogeneity.

Contributors

Lu-lu ZHANG designed the research. Yi-xuan SUN performed the analyses and wrote the first draft of the manuscript. Hao-qing YANG provided suggestions for improvement of analyses. Jie ZHANG, Zi-jun CAO, and Jun-yi YAN helped to organize the manuscript. Qi CUI and Yi-xuan SUN performed the lab model tests. Yi-xuan SUN and Lu-lu ZHANG revised and edited the final version.

Conflict of interest

Yi-xuan SUN, Lu-lu ZHANG, Hao-qing YANG, Jie ZHANG, Zi-jun CAO, Qi CUI, and Jun-yi YAN declare that they have no conflict of interest.

References

Ahmed AS, Jardani A, Revil A, et al., 2015. HT2DINV: a 2D forward and inverse code for steady-state and transient hydraulic tomography problems. *Computers & Geosciences*, 85:36-44. https://doi.org/10.1016/j.cageo.2015.08.009

Atkinson KE, 1967. The numerical solution of Fredholm integral equations of the second kind. *SIAM Journal on Numerical Analysis*, 4(3):337-348. https://doi.org/10.1137/0704029

Baecher GB, Christian JT, 2003. Reliability and Statistics in Geotechnical Engineering. John Wiley & Sons, Chichester, UK.

Bilgin Ö, Arens K, Dettloff A, 2019. Assessment of variability in soil properties from various field and laboratory tests. *Georisk: Assessment and Management of Risk for Engineered Systems and Geohazards*, 13(4):247-254. https://doi.org/10.1080/17499518.2019.1645338

Bowles JE, 1996. Foundation Analysis and Design, 5th Edition. McGraw-Hill, New York, USA.

Box GE, Tiao GC, 2011. Bayesian Inference in Statistical Analysis, Vol. 40. Wiley, New York, USA.

Cao ZJ, Wang Y, 2013. Bayesian approach for probabilistic site characterization using cone penetration tests. *Journal of Geotechnical and Geoenvironmental Engineering*, 139(2):267-276. https://doi.org/10.1061/(ASCE)GT.1943-5606.0000765

Chao WL, Wang XH, 2011. Research of mechanical parameter back analysis for the stratified soil slope. *Applied Mechanics and Materials*, 71-78:1893-1897. https://doi.org/10.4028/www.scientific.net/AMM.71-78.1893

Chen RH, Wu CP, Huang FC, et al., 2013. Numerical analysis of geocell-reinforced retaining structures. *Geotextiles and Geomembranes*, 39:51-62. https://doi.org/10.1016/j.geotexmem.2013.07.003

Chen Y, Zhang DX, 2006. Data assimilation for transient flow in geologic formations via ensemble Kalman filter. *Advances in Water Resources*, 29(8):1107-1122. https://doi.org/10.1016/j.advwatres.2005.09.007

Chowdhury R, Zhang S, Flentje P, 2004. Reliability updating and geotechnical back-analysis. *In*: Jardine RJ, Potts DM, Higgins KG (Eds.), Advances in Geotechnical Engineering: the Skempton Conference. Thomas Telford, London, UK, p.815-821.

Crisp MP, Jaksa MB, Kuo YL, et al., 2019. A method for generating virtual soil profiles with complex, multi-layer stratigraphy. *Georisk: Assessment and Management of Risk for Engineered Systems and Geohazards*, 13(2):154-163. https://doi.org/10.1080/17499518.2018.1554817

Dasaka SM, Zhang LM, 2012. Spatial variability of in situ weathered soil. *Géotechnique*, 62(5):375-384. https://doi.org/10.1680/geot.8.P.151.3786

Fenton GA, Griffiths DV, 2002. Probabilistic foundation settlement on spatially random soil. *Journal of Geotechnical and Geoenvironmental Engineering*, 128(5):381-390. https://doi.org/10.1061/(asce)1090-0241(2002)128:5(381)

Gavin K, Xue J, 2009. Use of a genetic algorithm to perform reliability analysis of unsaturated soil slopes. *Géotechnique*, 59(6):545-549. https://doi.org/10.1680/geot.8.T.004

Gelman A, Rubin DB, 1992. Inference from iterative simulation using multiple sequences. *Statistical Science*, 7(4):457-472. https://doi.org/10.1214/ss/1177011136

Ghanem RG, Spanos PD, 1991. Spectral stochastic finite-element formulation for reliability analysis. *Journal of Engineering Mechanics*, 117(10):2351-2372. https://doi.org/10.1061/(asce)0733-9399(1991)117:10(2351)

Ghanem RG, Spanos PD, 2003. Stochastic Finite Elements: a Spectral Approach. Courier Corporation, Massachusetts, USA.

Gilbert RB, Wright SG, Liedtke E, 1998. Uncertainty in back analysis of slopes: Kettleman hills case history. *Journal of Geotechnical and Geoenvironmental Engineering*, 124(12):1167-1176. https://doi.org/10.1061/(asce)1090-0241(1998)124:12(1167)

Huang SP, Quek ST, Phoon KK, 2001. Convergence study of the truncated Karhunen–Loeve expansion for simulation

of stochastic processes. *International Journal for Numerical Methods in Engineering*, 52(9):1029-1043. https://doi.org/10.1002/nme.255

Huang SP, Mahadevan S, Rebba R, 2007. Collocation-based stochastic finite element analysis for random field problems. *Probabilistic Engineering Mechanics*, 22(2):194-205. https://doi.org/10.1016/j.probengmech.2006.11.004

Ishii Y, Ota K, Kuraoka S, et al., 2012. Evaluation of slope stability by finite element method using observed displacement of landslide. *Landslides*, 9(3):335-348. https://doi.org/10.1007/s10346-011-0303-7

Jiang SH, Li DQ, Zhang LM, et al., 2014. Slope reliability analysis considering spatially variable shear strength parameters using a non-intrusive stochastic finite element method. *Engineering Geology*, 168:120-128. https://doi.org/10.1016/j.enggeo.2013.11.006

Jiang SH, Li DQ, Cao ZJ, et al., 2015. Efficient system reliability analysis of slope stability in spatially variable soils using Monte Carlo simulation. *Journal of Geotechnical and Geoenvironmental Engineering*, 141(2):04014096. https://doi.org/10.1061/(ASCE)GT.1943-5606.0001227

Jiang SH, Papaioannou I, Straub D, 2018. Bayesian updating of slope reliability in spatially variable soils with in-situ measurements. *Engineering Geology*, 239:310-320. https://doi.org/10.1016/j.enggeo.2018.03.021

Jin YF, Yin ZY, Shen SL, et al., 2016. Selection of sand models and identification of parameters using an enhanced genetic algorithm. *International Journal for Numerical and Analytical Methods in Geomechanics*, 40(8):1219-1240. https://doi.org/10.1002/nag.2487

Jin YF, Yin ZY, Shen SL, et al., 2017. A new hybrid real-coded genetic algorithm and its application to parameters identification of soils. *Inverse Problems in Science and Engineering*, 25(9):1343-1366. https://doi.org/10.1080/17415977.2016.1259315

Jin YF, Yin ZY, Wu ZX, et al., 2018. Identifying parameters of easily crushable sand and application to offshore pile driving. *Ocean Engineering*, 154:416-429. https://doi.org/10.1016/j.oceaneng.2018.01.023

Jin YF, Yin ZY, Zhou WH, et al., 2019a. Bayesian model selection for sand with generalization ability evaluation. *International Journal for Numerical and Analytical Methods in Geomechanics*, 43(14):2305-2327. https://doi.org/10.1002/nag.2979

Jin YF, Yin ZY, Zhou WH, et al., 2019b. Identifying parameters of advanced soil models using an enhanced transitional Markov chain Monte Carlo method. *Acta Geotechnica*, 14(6):1925-1947. https://doi.org/10.1007/s11440-019-00847-1

Jin YF, Yin ZY, Zhou WH, et al., 2019c. Multi-objective optimization-based updating of predictions during excavation. *Engineering Applications of Artificial Intelligence*, 78:102-123. https://doi.org/10.1016/j.engappai.2018.11.002

Karhunen K, 1947. Über lineare methoden in der wahrscheinlichkeitsrechnung. *Annales Academiae Scientiarum Fennicae*, 37:1-79 (in German).

Ledesma A, Gens A, Alonso EE, 1996. Parameter and variance estimation in geotechnical backanalysis using prior information. *International Journal for Numerical and Analytical Methods in Geomechanics*, 20(2):119-141. https://doi.org/10.1002/(SICI)1096-9853(199602)20:2<119::AID-NAG810>3.0.CO;2-L

Lee KZZ, Chang NY, 2012. Predictive modeling on seismic performances of geosynthetic-reinforced soil walls. *Geotextiles and Geomembranes*, 35:25-40. https://doi.org/10.1016/j.geotexmem.2012.06.005

Leshchinsky B, Ling HI, 2013. Numerical modeling of behavior of railway ballasted structure with geocell confinement. *Geotextiles and Geomembranes*, 36:33-43. https://doi.org/10.1016/j.geotexmem.2012.10.006

Li DQ, Qi XH, Phoon KK, et al., 2014. Effect of spatially variable shear strength parameters with linearly increasing mean trend on reliability of infinite slopes. *Structural Safety*, 49:45-55. https://doi.org/10.1016/j.strusafe.2013.08.005

Li DQ, Jiang SH, Cao ZJ, et al., 2015. A multiple response-surface method for slope reliability analysis considering spatial variability of soil properties. *Engineering Geology*, 187:60-72. https://doi.org/10.1016/j.enggeo.2014.12.003

Li JH, Zhang LM, 2011. Study of desiccation crack initiation and development at ground surface. *Engineering Geology*, 123(4):347-358. https://doi.org/10.1016/j.enggeo.2011.09.015

Li JH, Zhou Y, Zhang LL, et al., 2016. Random finite element method for spudcan foundations in spatially variable soils. *Engineering Geology*, 205:146-155. https://doi.org/10.1016/j.enggeo.2015.12.019

Li YH, Zhang Q, Lin ZB, et al., 2016. Spatiotemporal evolution rule of rocks fracture surrounding gob-side roadway with model experiments. *International Journal of Mining Science and Technology*, 26(5):895-902. https://doi.org/10.1016/j.ijmst.2016.05.031

Liu K, Vardon PJ, Hicks MA, 2018. Sequential reduction of slope stability uncertainty based on temporal hydraulic measurements via the ensemble Kalman filter. *Computers and Geotechnics*, 95:147-161. https://doi.org/10.1016/j.compgeo.2017.09.019

Loève M, 1948. Fonctions Aléatoires de Second Ordre. Supplement to P. Levy, Proces Stochastiques et Mouvement Brownien. Gauthier-Villars, Paris, France (in French).

Mavritsakis A, 2017. Evaluation of Inverse Analysis Methods with Numerical Simulation for Slope Excavation. MS Thesis, Delft University of Technology, Delft, the Netherland.

Novák V, Šimůnek J, van Genuchten MT, 2000. Infiltration of water into soil with cracks. *Journal of Irrigation and Drainage Engineering*, 126(1):41-47. https://doi.org/10.1061/(asce)0733-9437(2000)126:1(41)

Pan QJ, Qu XR, Liu LL, et al., 2020. A sequential sparse polynomial chaos expansion using Bayesian regression for geotechnical reliability estimations. *International Journal for Numerical and Analytical Methods in Geomechanics*, 44(6):874-889. https://doi.org/10.1002/nag.3044

Phoon KK, Kulhawy FH, 1999a. Characterization of geotechnical variability. *Canadian Geotechnical Journal*, 36(4):612-624. https://doi.org/10.1139/t99-038

Phoon KK, Kulhawy FH, 1999b. Evaluation of geotechnical property variability. *Canadian Geotechnical Journal*, 36(4): 625-639. https://doi.org/10.1139/t99-039

Phoon KK, Tang C, 2019. Characterisation of geotechnical model uncertainty. *Georisk: Assessment and Management of Risk for Engineered Systems and Geohazards*, 13(2):101-130. https://doi.org/10.1080/17499518.2019.1585545

Qi XH, Li DQ, 2018. Effect of spatial variability of shear strength parameters on critical slip surfaces of slopes. *Engineering Geology*, 239:41-49. https://doi.org/10.1016/j.enggeo.2018.03.007

Smolyak SA, 1963. Quadrature and interpolation formulae on tensor products of certain function classes. *Doklady Akademii Nauk SSSR*, 4(5):1042-1045.

Sun HY, Wang J, Wang DF, et al., 2020. Optimal design of prefabricated vertical drain-improved soft ground considering uncertainties of soil parameters. *Journal of Zhejiang University-SCIENCE A (Applied Physics & Engineering)*, 21(1):15-28. https://doi.org/10.1631/jzus.A1900227

Tang WH, Ang AHS, 2007. Probability Concepts in Engineering: Emphasis on Applications in Civil & Environmental Engineering, 2nd Edition. John Wiley & Sons, New York, USA.

Vardon PJ, Liu K, Hicks MA, 2016. Reduction of slope stability uncertainty based on hydraulic measurement via inverse analysis. *Georisk: Assessment and Management of Risk for Engineered Systems and Geohazards*, 10(3): 223-240. https://doi.org/10.1080/17499518.2016.1180400

Vrugt JA, ter Braak CJF, Clark MP, et al., 2008. Treatment of input uncertainty in hydrologic modeling: doing hydrology backward with Markov Chain Monte Carlo simulation. *Water Resources Research*, 45(12):W00B09. https://doi.org/10.1029/2007WR006720

Wang L, Hwang JH, Luo Z, et al., 2013. Probabilistic back analysis of slope failure–a case study in Taiwan. *Computers and Geotechnics*, 51:12-23. https://doi.org/10.1016/j.compgeo.2013.01.008

Xiao J, Liu G, Liu J, et al., 2019. Parameters of a discrete element ballasted bed model based on a response surface method. *Journal of Zhejiang University-SCIENCE A (Applied Physics & Engineering)*, 20(9):685-700. https://doi.org/10.1631/jzus.A1900133

Xiu DB, 2007. Efficient collocational approach for parametric uncertainty analysis. *Communications in Computational Physics*, 2(2):293-309.

Yan L, Meng QX, Xu WY, et al., 2017. A numerical method for analyzing the permeability of heterogeneous geomaterials based on digital image processing. *Journal of Zhejiang University-SCIENCE A (Applied Physics & Engineering)*, 18(2):124-137. https://doi.org/10.1631/jzus.A1500335

Yang HQ, Zhang LL, Li DQ, 2018. Efficient method for probabilistic estimation of spatially varied hydraulic properties in a soil slope based on field responses: a Bayesian approach. *Computers and Geotechnics*, 102: 262-272. https://doi.org/10.1016/j.compgeo.2017.11.012

Yang HQ, Zhang LL, Xue JF, et al., 2019. Unsaturated soil slope characterization with Karhunen-Loève and polynomial chaos via Bayesian approach. *Engineering with Computers*, 35(1):337-350. https://doi.org/10.1007/s00366-018-0610-x

Yang HQ, Chen XY, Zhang LL, et al., 2020. Conditions of hydraulic heterogeneity under which Bayesian estimation is more reliable. *Water*, 12(1):160. https://doi.org/10.3390/w12010160

Yang J, Yin ZY, Laouafa F, et al., 2019a. Analysis of suffusion in cohesionless soils with randomly distributed porosity and fines content. *Computers and Geotechnics*, 111: 157-171. https://doi.org/10.1016/j.compgeo.2019.03.011

Yang J, Yin ZY, Laouafa F, et al., 2019b. Internal erosion in dike-on-foundation modeled by a coupled hydromechanical approach. *International Journal for Numerical and Analytical Methods in Geomechanics*, 43(3):663-683. https://doi.org/10.1002/nag.2877

Yin ZY, Jin YF, Shen SL, et al., 2017. An efficient optimization method for identifying parameters of soft structured clay by an enhanced genetic algorithm and elastic-viscoplastic model. *Acta Geotechnica*, 12(4):849-867. https://doi.org/10.1007/s11440-016-0486-0

Zhang J, Tang WH, Zhang LM, 2010. Efficient probabilistic back-analysis of slope stability model parameters. *Journal of Geotechnical and Geoenvironmental Engineering*, 136(1):99-109. https://doi.org/10.1061/(ASCE)GT.1943-5606.0000205

Zhang J, Zhou CW, Jia C, et al., 2017. Powell inversion mechanical model of foundation parameters with generalized Bayesian theory. *Journal of Zhejiang University-SCIENCE A (Applied Physics & Engineering)*, 18(7): 567-578. https://doi.org/10.1631/jzus.A1600440

Zhang LL, Zhang J, Zhang LM, et al., 2010. Back analysis of slope failure with Markov Chain Monte Carlo simulation. *Computers and Geotechnics*, 37(7-8):905-912. https://doi.org/10.1016/j.compgeo.2010.07.009

Zhang LL, Zuo ZB, Ye GL, et al., 2013. Probabilistic parameter estimation and predictive uncertainty based on field

measurements for unsaturated soil slope. *Computers and Geotechnics*, 48:72-81. https://doi.org/10.1016/j.compgeo.2012.09.011

Zhang LL, Zheng YF, Zhang LM, et al., 2014. Probabilistic model calibration for soil slope under rainfall: effects of measurement duration and frequency in field monitoring. *Géotechnique*, 64(5):365-378. https://doi.org/10.1680/geot.13.P.134

Zhang LL, Li JH, Li X, et al., 2016. Rainfall-induced Soil Slope Failure: Stability Analysis and Probabilistic Assessment. CRC Press, Taylor & Francis Group, Boca Raton, USA.

Zhang SR, Hu AK, Wang C, 2016. Three-dimensional inversion analysis of an in situ stress field based on a two-stage optimization algorithm. *Journal of Zhejiang University-SCIENCE A (Applied Physics & Engineering)*, 17(10):782-802. https://doi.org/10.1631/jzus.A1600014

中文概要

题　目：基于观测响应的土体空间变异性表征：位移反分析应用

目　的：由于现场勘察和室内土工试验数据的不足，因此土体空间变异性难以估计。通过间接方法如反演分析方法进行估算是一个有效的途径，而土体参数空间变异性概率反演估计的准确性受变异特性自身影响。本文旨在通过算例研究和模型试验验证，明确影响土体空间变异性反演准确性的关键因素，以期为岩土勘察测试工程实践提供参考。

创新点：1. 通过土坡空间变异性反演分析，揭示数据类型、变异系数、相关长度和协方差函数类型等对反演的影响；2. 室内分层土模型试验验证表明，概率反演分析方法可有效地识别土体层厚和内摩擦角变异性。

方　法：1. 通过边坡数值算例，研究位移监测数据类型、土体相关长度、弹性模量变异系数以及协方差函数对弹性模量空间变异性的位移反分析的影响（图 5、6、9、11 和 12）。2. 开展室内模型试验，利用粒子图像测试技术获取位移监测数据，对分层土体内摩擦角的变异性进行识别，并研究软弱夹层位置与厚度对反分析的影响（图 14）。

结　论：1. 水平位移比竖直位移更适合用于位移反分析。2. 反分析精度在可接受范围内，且对于高变异性的情况（COV_E=1.5），误差不超过 10%；此外，反分析精度还受协方差函数类型和相关长度的影响。3. 反分析可识别出模型试验的土体分层，并且对内摩擦角的估计误差小于 10%。

关键词：土体空间变异性；概率估计；位移；相关长度；模型试验